Nuclear Inst. and Methods in Physics Research, A 916 (2019) 230–237

Contents lists available at ScienceDirect

Nuclear Inst. and Methods in Physics Research, A

journal homepage: www.elsevier.com/locate/nima

CLIC380: RF design and parameters of 2017 re-baselined 380 GeV CLIC linac accelerating structure

Xiaoxia Huang [a,b,c], Alexej Grudiev [c], Zhentang Zhao [a,b], Wencheng Fang [a,*]

[a] Shanghai Institute of Applied Physics, Chinese Academy of Sciences, Shanghai 201800, China
[b] University of Chinese Academy of Sciences, Beijing 100049, China
[c] CERN, European Organization for Nuclear Research, Geneva 1211, Switzerland

ARTICLE INFO

Keywords:
Waveguide-damped structure
Waveguide opening
Forth order polynomial function
Transverse wakefield suppression

ABSTRACT

This work presents an optimized damping waveguide structure designed to satisfy the radio frequency parameters and long-range transverse wakefield suppression of the 380 GeV Compact Linear Collider facility currently under study. Here, the elliptical shape of the iris and the wall shape of the damping waveguides are both optimized to reduce the magnitudes of surface electromagnetic fields. The widths of the waveguide openings of the entire sequence of damping waveguides are also decreased linearly with respect to the direction of beam propagation to strongly suppress long-range transverse wakefields and to maintain the stability of the beam. The position of the high-order-mode damping loads in the waveguide structure is also studied to make the damping waveguide structure more compact while satisfying all design targets.

1. Introduction

The Compact Linear Collider (CLIC) is a very large-scale electron linear accelerator facility that is currently under study by the European Organization for Nuclear Research (CERN). The CLIC facility is envisioned as a three-stage accelerator that aims to achieve a 3 TeV center-of-mass collision energy in the final stage [1]. In particular, the first stage of the accelerator structure, denoted as the CLIC380, is envisioned to accelerate electron and positron beams up to a center-of-mass collision energy of 380 GeV with an average acceleration gradient of 72 MV/m [2]. The CLIC380 structure is composed of 31 damping waveguide cells and two couplers. As illustrated in Fig. 1, a damping waveguide cell is composed of four waveguides that are each terminated by damping structures (i.e., damping loads) for absorbing high-order modes (HOMs). The damping cell geometry is designed to limit the effect of the HOM damping loads on the beam and to suppress long-range transverse wakefields. However, the CLIC380 is an X-band $2\pi/3$ mode structure with a fundamental frequency $f = 11.994$ GHz. The dimension of the structure is relatively small, and the wakefield effect is strong. Moreover, the CLIC380 functions in the multi-bunch operation mode, and the beam stability in this mode is affected strongly by long-range transverse wakefields, which makes the maintenance of beam stability problematic, and therefore increases the possibility of beam collapse. Thus, the CLIC380 structure requires suppression of the magnitudes of both surface electromagnetic fields and long-range transverse wakefields.

This work seeks to address these issues associated with the CLIC380 structure by optimizing the design of the damping waveguide cell. To reduce the magnitudes of surface electromagnetic fields, we have optimized both the elliptical shape of the iris and the wall shape of the damping waveguides. Meanwhile, in order to strongly suppress long-range transverse wakefields and maintain the stability of the beam, we adopt linearly decreasing on the widths of the waveguide openings of the entire sequence of damping waveguides in the direction of beam propagation. We also studied on the position of the HOM damping loads in the waveguide structure to make the damping waveguide structure more compact while satisfying all design targets. For the CLIC380 structure, the transverse kick should be below 3.4 V/pC/m/mm at the distance between each two bunches. A new enhance factor is introduced to diagnose the multi-bunch enhancement on transverse wakefields, which is detail discussed at third section. Meanwhile the enhance factor is below 5 and the temperature rise is less than 40 K.

2. Geometry of the damping waveguide cell

A number of performance parameters must be considered in the design of the damping waveguide cell. Among the parameters illustrated in Fig. 2, the radius of the iris aperture a and the thickness of the iris d are crucial geometrical parameters that affect the group velocity, radio frequency (RF) efficiency and wakefield characteristics of the beam [3]. However, the values of a and d in the design of the CLIC380 have been fixed by global optimization of beam dynamics [2]. The values of a are

* Corresponding author.
E-mail addresses: Alexej.Grudiev@cern.ch (A. Grudiev), fangwencheng@sinap.ac.cn (W. Fang).

https://doi.org/10.1016/j.nima.2018.11.104
Received 21 August 2018; Received in revised form 8 November 2018; Accepted 21 November 2018
Available online 27 November 2018

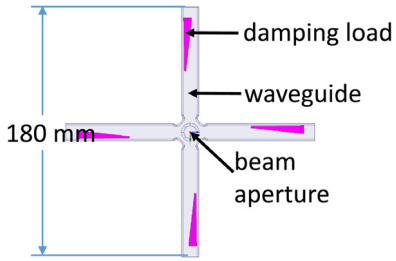

Fig. 1. Schematic of a damping waveguide cell composed of four waveguides perpendicular to the direction of beam propagation and terminated by damping structures (i.e., damping loads) for application in the CLIC380 accelerating structure.

linearly decreased from 4.062 mm to 2.600 mm and the values of d are linearly decreased from 2.525 mm to 1.433 mm. Nonetheless, the width of the waveguide opening iw and the waveguide width w are important free parameters that can be adjusted for optimizing the design of the damping waveguide cell. In addition, the shape factor e of the elliptical iris, which is illustrated in the longitudinal section of the iris in Fig. 2, is variable, and the radius of the cavity b is adjusted to meet the 11.994 GHz frequency requirement. All other parameters can be set as constant values in every cell.

The gradient and breakdown rate are important parameters for the CLIC380. High power tests have demonstrated that the maximum gradient in an undamped structure is typically about 10%–20% greater than that of a damped structure [4]. As shown in Fig. 3, the maximum gradient is limited by the surface electromagnetic field, and can be modified by adjusting the Poynting vector Sc [5] and the temperature increase ΔT at the cell wall due to pulse surface heating. The maximum value of Sc is at the iris tip, and the maximum value of the magnetic field Hs, which is used to calculate ΔT, occurs at the cell wall. The values of Sc and Hs must be maintained below specific thresholds to ensure that the CLIC380 structure can be operated under a nominal breakdown rate of 3×10^{-7} breakdowns per pulse per meter. A relatively simple means of achieving this requirement is to optimize the geometrical shapes of the iris and the cell wall. Here, the distribution of Sc along the iris edge is largely dependent on the value of e, where an optimal e provides a Sc distribution along the iris edge with a flattened top at the iris tip. The optimal geometrical shape of the cell wall can be determined by adopting the following fourth order polynomial function [6]:

$$Y = Y_0 + (X - X_0) + \left(\frac{X}{X_0} - 1\right)^2 \left(A_0 + A_1 \frac{X}{X_0} + A_2 \frac{X^2}{X_0}\right) \tag{1}$$

where $Y_0 = \frac{b}{\sqrt{2}} - \frac{iw}{2}$, $X_0 = A_0 + Y_0$ and $A_1 = A_0 - Y_0$. Here, an optimal selection of A_0, A_2, b and iw can remove irregularities in the distribution of Hs, and thereby control the pulse surface heating. This discussion is illustrated by plots of the Sc obtained along the iris edge with different values of e shown in Fig. 4(a), and plots of the Hs obtained along the cell wall with different values of A_0 and A_2 shown in Fig. 4(b) using ANSYS HFSS software [7]. The results demonstrate that the maximum values of Sc and Hs are reduced by 2.3% and 2.7%, respectively, when employing optimal parameters. The reduction in Hs represents a decrease in ΔT of 1.4 K.

3. Transverse wakefield potentials

Long-range transverse wakefields can be calculated using the commercial wakefield simulation software GdfidL [8]. The accuracy of this software has been verified by comparing calculated results with experimental measurements [9]. The transverse wakefield suppression in the damping waveguide structure of the CLIC380 is influenced by iw and w simultaneously. In the analysis of transverse wakefields, the transverse wakefield potentials W_T at two points along the beam direction s are of particular importance. The first W_T value of interest is the transverse wakefield potential at the distance $s = 0.15$ m, which is the distance associated with the standard bunch separation of 6 RF cycles at $f = 11.994$ GHz (i.e., 0.5 ns). The second W_T value of interest is the bigger one of absolute envelope value of the transverse wakefield potential peaks nearest to $s = 0.15$ m. The requirement is that these two transverse wakefield potential W_T values of interest are less than 3.4 V/pC/m/mm. In terms of the optimization of transverse wakefield suppression based on iw and w, Fig. 5(a) shows that, if the value of w is fixed at 10.7 mm, the extent of wakefield suppression increases at $s = 0.15$ m with increasing iw. In contrast, Fig. 5(b) shows that, if the value of iw is fixed at 8.6 mm, an optimal value of w obtains a minimum peak transverse wakefield magnitude nearby $s = 0.15$ m.

However, long-range wakefields exert an effect not only between adjacent bunches but also over multiple bunches. For the CLIC380, the number of bunches N_b is 352, and the number of electrons per bunch N_e is 5.2×10^9. Assuming that any bunch has an effect on subsequent bunches, we define the effect of bunch k on a subsequent bunch j as a_{jk}. However, we must also consider the multi-bunch regime, where bunches prior to bunch k generate a chain reaction of effects. Accordingly, we define the final effect of bunch k on bunch j as A_{jk}. The values of a_{jk} and the matrix $\mathbf{A}$ composed of the elements A_{jk} are defined as follows:

$$\begin{aligned} a_{jk} &= \begin{cases} C \cdot W_T\left(z_{j-k}\right) \cdot N_e {q_e}^2 & , j > k \\ 0 & , j \le k \end{cases} \\ A &= e^a = \sum_{m=0}^{N_b} \frac{(i \cdot a)^m}{m!} \end{aligned} \tag{2}$$

Here, C is a constant coefficient, W_T is the transverse wakefield potential, z_{j-k} is the position along the beam axis between bunches k and j, q_e is the electron charge and i is imaginary number. To ensure beam stability, a parameter F_{rms} as formula (3) is introduced to characterize the transverse wakefield enhancement caused by beam jitter [10]. For F_{rms}, we note that this is calculated using the maximum of the absolute values of the two transverse wakefield potential values of interest defined previously. The values of W_T calculated using GdfidL are shown in Fig. 6, where the interval between adjacent vertical lines is the distance between two bunches. The points of intersection are corresponding to $W_T(z_{j-k})$, for F_{rms} calculation. In this design, $C = 190$ m^2 GeV^{-1} according to the linac layout, energy and acceleration gradient. In addition, F_{rms} is required to be less than 5 to keep the main CLIC380 linac stable in the ensuing discussion.

$$F_{rms} = \frac{1}{N_b} \sum_{j=1}^{N_b} \sum_{k=1}^{j} \left|A_{jk}\right|^2 \tag{3}$$

4. Tapered CLIC380 structure

The simulation model for the CLIC380 structure is shown in Fig. 7. The structure includes 31 regular damping cells and two matched coupling cells with an equivalent design as that of the damping cells. In addition, the values of the parameters a and d decrease linearly along the direction of beam propagation, and the same w and iw are used to simulate transverse wakefields firstly. The values of W_T calculated for the simulation model given in Fig. 7 with the different values of iw and w using GdfidL are shown in Fig. 8. The value of F_{rms} corresponds to the envelope of W_T, which is greater than the value of W_T calculated at $s = z_{j-k}$ and must be less than the stability criterion of 5. The results in Fig. 8 indicate that values of $w = 10.7$ mm and $iw > 8.5$ mm meet both the W_T and F_{rms} criteria requirements.

However, the values of iw and w are also related to the magnitudes of surface fields. As such, the relatively large value of iw required to ensure that the value of F_{rms} is less than the criterion value also results in higher Sc and Hs, and correspondingly higher values of ΔT. This is particularly problematic because the value of ΔT increases from the first cell to the last cell in the CLIC380 structure. For example, the simulation model given in Fig. 7 with $w = 10.7$ mm and constant iw of each cell increased from 8.2 mm to 8.9 mm increases the maximum value of ΔT

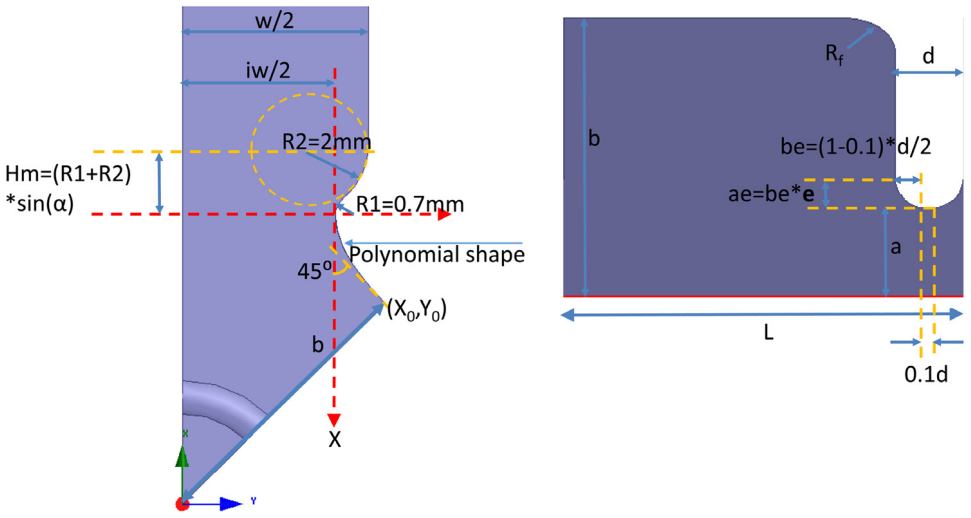

Fig. 2. Geometry of the damping waveguide cell.

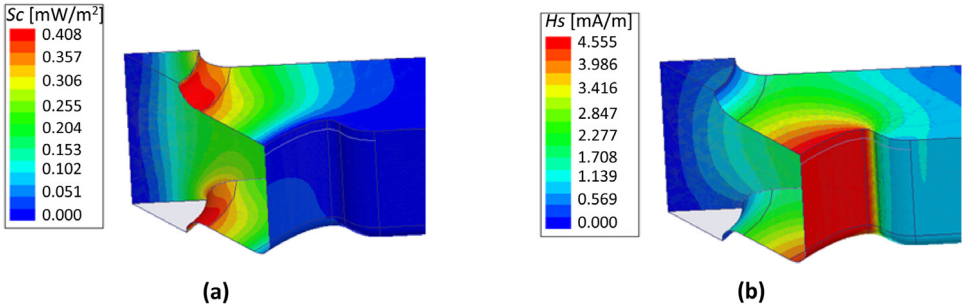

Fig. 3. Electromagnetic field distribution on the surface of the CLIC380 when average gradient is 1 V/m: (a) Poynting vector *Sc*; (b) magnetic field *Hs*.

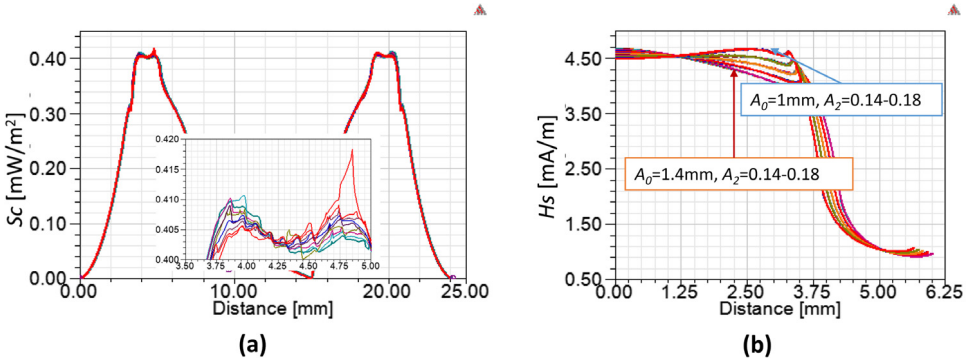

Fig. 4. Simulated electromagnetic field distributions when average gradient is 1 V/m: (a) *Sc* along the iris edge with different values of *e* ranging from 1.46 to 1.54 in steps of 0.01; (b) *Hs* along the cell wall with different values of A_0 ranging from 1 mm to 1.4 mm in steps of 0.1 mm and A_2 ranging from 0.14 to 0.18 in steps of 0.01.

from 39 K to 50 K. Therefore, the next step is to optimize the design to obtain maximum transverse wakefield suppression while maintaining a sufficiently low ΔT. This can be addressed by varying the values of *iw* in each cell, rather than holding them constant. As shown in Fig. 9, applying a linearly decreasing *iw* with $w = 10.7$ mm can effectively reduce ΔT while maintaining W_T and F_{rms} under their required limits. In particular, we note that adjusting the value of *iw* in the last cell reduces the maximum value of ΔT to less than 40 K.

Through adjusting the value of *iw* in last cell, the maximum temperature rise is reduced below 40 K. If the average *iw* is the same, the smaller *iw* is in last cell, the smaller ΔT, W_T and F_{rms} are in tapered structure, shown in Fig. 10. The solid lines are the results of average *iw* = 8.6 mm, and the dashed lines are that of *iw* = 8.7 mm. All results are normalized to the results (ΔT, W_T, F_{rms}) of constant *iw* distribution with 8.6 mm. The maximum ΔT is mainly determined by the *iw* of last cell. Meanwhile, reducing *iw* of downstream cell means increasing that of upstream cell, which achieve stronger wakefield suppression in overall effects.

If the average *iw* is the same, the smaller *iw* is in last cell, the smaller ΔT, W_T and F_{rms} are in tapered structure, shown in Fig. 10. All results in Fig. 10 are normalized according to the values of ΔT, W_T and F_{rms} obtained for the simulation model in Fig. 7 with a constant value of *iw* = 8.6 mm. The solid lines are the results of an average *iw* = 8.6 mm and the dashed lines are that of an average *iw* = 8.7 mm. The maximum ΔT is mainly determined by the *iw* value of the last cell. Meanwhile, reducing the value of *iw* downstream corresponds to increasing the value of *iw* upstream, which achieves an overall stronger wakefield suppression

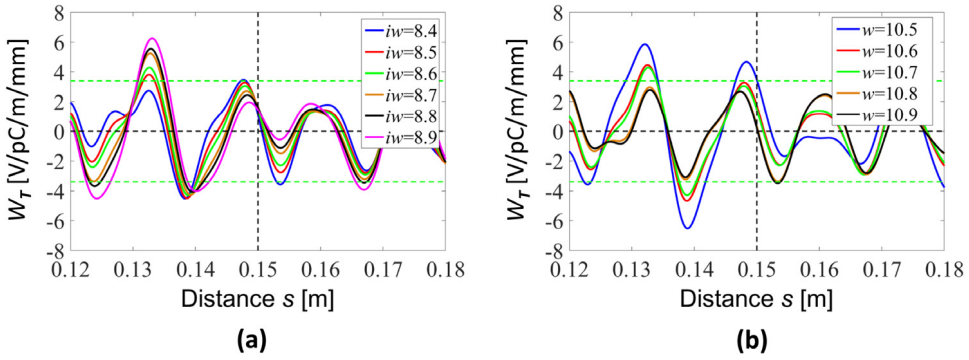

Fig. 5. Magnitude of transverse wakefields W_T for different waveguide opening widths *iw* and waveguide widths *w*, where *s* is the distance between two adjacent bunches and the W_T values of green lines are ±3.4 V/pC/m/mm: (a) as a function of *iw* with *w* fixed at 10.7 mm, (b) as a function of *w* with *iw* fixed at 8.6 mm.

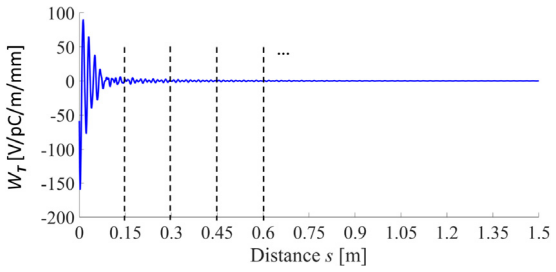

Fig. 6. Transverse wakefield potential W_T distribution between bunches where z_{j-k}, j-k = 1, 2, …, N_b.

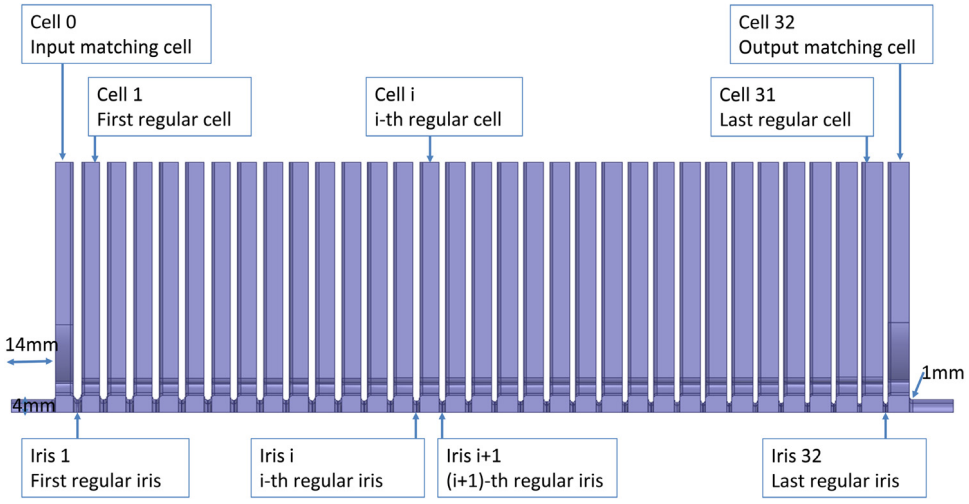

Fig. 7. The simulation model of tapered structure.

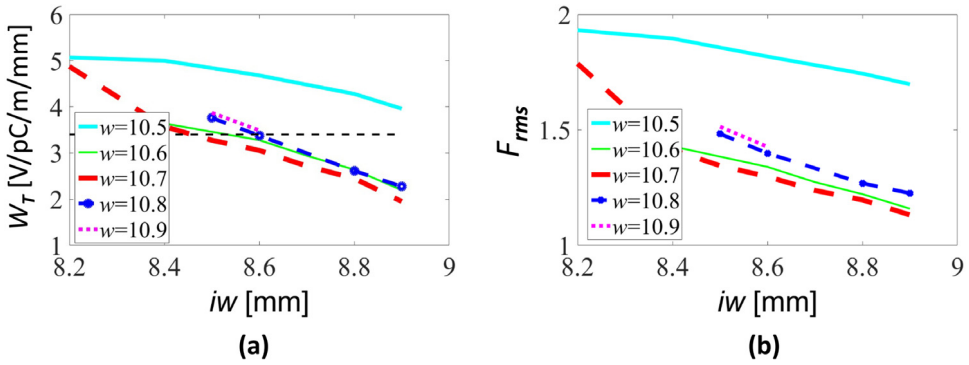

Fig. 8. Transverse wakefield potentials W_T obtained with the simulation model given in Fig. 7 for different values of *iw* and *w*: (a) W_T at two adjacent bunches (s = 0.15 m), where the dashed line is the stability criterion (3.4 V/pC/m/mm); (b) F_{rms} distribution with the stability criterion of 5.

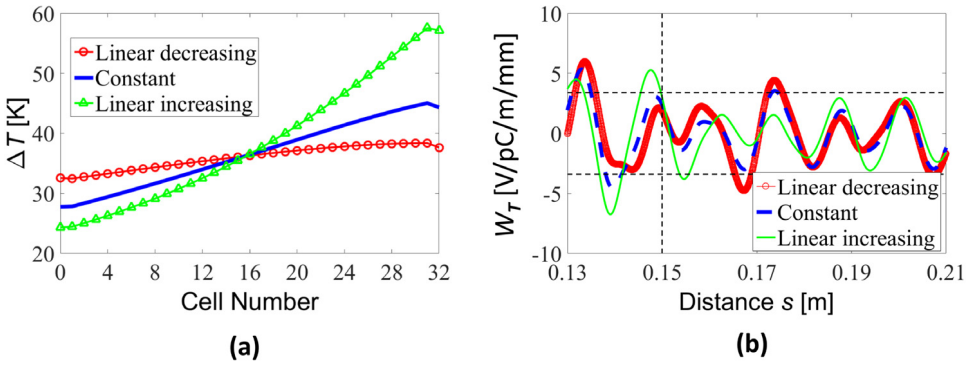

Fig. 9. Temperature increase ΔT in each cell due to pulse surface heating and W_T obtained with the simulation model given in Fig. 7 for three different distributions of *iw*: (a) ΔT and (b) W_T.

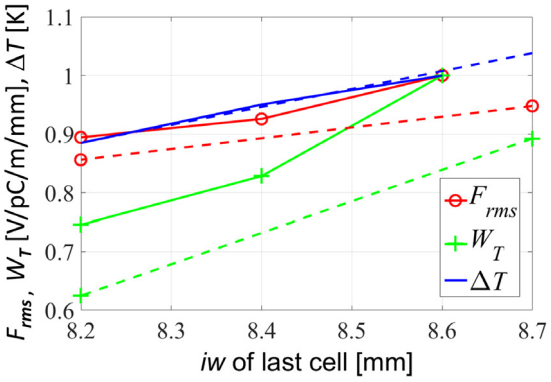

Fig. 10. Normalized values of ΔT, W_T and F_{rms} obtained in the last cell with different linearly decreasing distributions of *iw*.

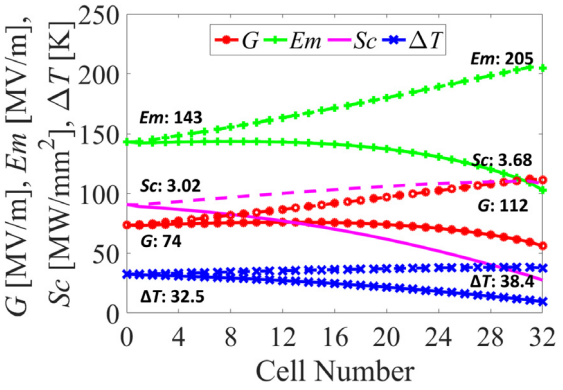

Fig. 11. Radio frequency (RF) parameters in the optimum CLIC380 structure.

Table 1
The parameters of all regular damping cells.

Frequency, f	11.994 GHz
Phase advance	$2\pi/3$
Cell No.	31
Cell length, L	8.332 mm
Iris thickness, d	2.525–1.433 mm
Aperture, a	4.062–2.600 mm
Waveguide opening, *iw*	9.200–8.200 mm
Waveguide width, w	10.7 mm
Shape of cell wall, A_0	1.149–1.072 mm
Shape of cell wall, A_2	0.15
Ratio of elliptic radius, e	1.521–1.470
Diameter, $2b$	17.537–16.888 mm

effect. Accordingly, *iw* = 8.2 mm in the last cell and *iw* = 9.2 mm in the first cell are applied to the design.

The tapered structure shown in Fig. 7 can be further optimized by adjusting the values of e, A_0 and A_2 to optimize the surface fields in the first cell, middle cell and last cell, respectively. The detailed parameters of all regular damping cells are listed in Table 1 [11]. The results are plotted in Fig. 11, where the filling time was 55.4 ns. Under the condition of beam loading, the input RF power should be 59.7 MW to achieve the designated load acceleration gradient target G = 72 MV/m. In the figure, the solid lines represent results obtained under the condition of beam loading with an input RF power of 59.7 MW and the dashed lines represent results obtained under the condition of no beam loading with the same input RF power. The value of E_m represents the maximum electric field magnitude of each cell obtained along the iris curve. Every cell has its own corresponding parameters of G, *Em*, *Sc* and ΔT along the CLIC380 structure plotted in Fig. 7. In Fig. 11, the minimum values and the maximum values of G, *Em*, *Sc* and ΔT are given with the beam loading unconsidered. The maximum value of ΔT is 38.4 K and that of *Sc* is 3.68 MW/mm^2. The output RF power values obtained are 27.6 MW and 6.2 MW under conditions of no loading and loading, respectively. The efficiency of RF power to beam power conversion is about 40%.

5. Coupler structure

The input and output RF power couplers are another important feature in the acceleration structure of the CLIC380. These components are responsible for ensuring power transmission from the standard waveguides to and from the tapered structure. The input coupler is positioned prior to the first damping cell in the position of the input matching cell shown in Fig. 7, and the output coupler is positioned at the end of the tapered structure. The CLIC380 design with couplers and the coupler geometry are illustrated in Fig. 12. This is a dual-feed geometry that is beneficial for eliminating the dipole component of the field. According to the optimized results, the values of *iw* are 9.2 mm and 8.2 mm for the first and last damping cells, respectively, which must be matched with the input coupler and output coupler, respectively. In addition, the width of the coupler waveguide opening *icw* and the cavity radius *b* affect the matching between the coupler and the damping cells. Adjusting these parameters carefully can ensure that the transmission coefficients from the input coupler to the first damping cell and from the last damping cell to the output coupler are nearly equal to 1, which ensures the absence of a reflection wave in the CLIC380 structure owing to an unmatched output coupler, which effects the simulated value S11 of port reflection at the input coupler. The matched results obtained by adjusting the values of *icw* and *b* for the couplers are shown in Fig. 13(a). Here, S11 is less than −50 dB at the operating frequency that the S11 parameter of the overall structure in this case is considered to be produced only by the input coupler. In this matched couplers case, the

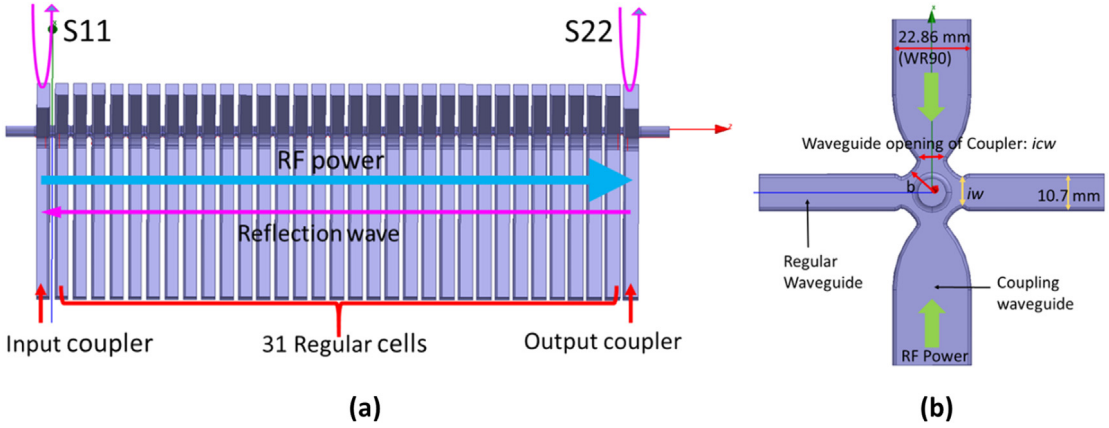

Fig. 12. (a) A quarter of the tapered CLIC380 structure with couplers. (b) Coupler geometry.

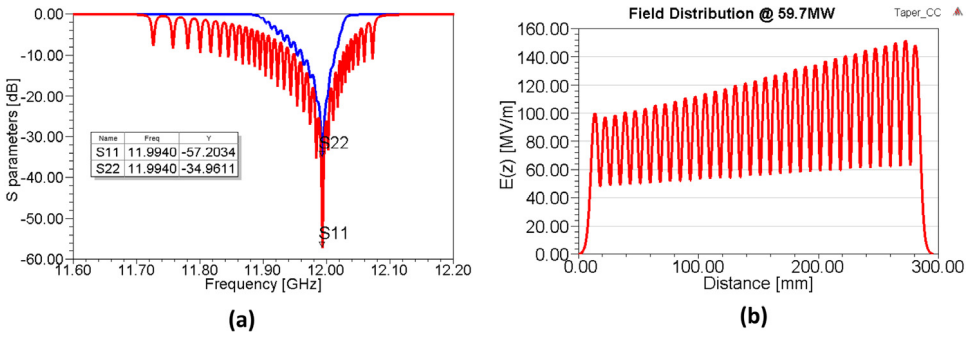

Fig. 13. The matched couplers results: (a) S parameters at different frequencies; (b) Simulated field distribution along the beam axis of the CLIC380 structure.

electric field distribution along the beam axis of the tapered structure is shown in Fig. 13(b).

In the matched case, we also can obtain the complex valued $E(z)$ along the beam axis of the tapered structure, which comprises the effects of forward waves and reflection waves (i.e., backward waves). The $E(z)$ can be defined as follows and satisfy the requirements:

$$\begin{aligned} &E(z) = E_0(z) \cdot \left(e^{-i\phi(z)} + R \cdot e^{i\phi(z)}\right) \\ &E_0(z \pm L) = E_0(z)\ ,\ \phi(z \pm L) = \phi(z) \pm \Psi \end{aligned} \tag{4}$$

where $E_0(z)$ is a real positive amplitude, $\phi(z)$ is the corresponding phase, and Ψ is the phase advance between cells in the CLIC380 design, which is 120° per cell with a period $L = 8.3316$ mm. The R is the reflection coefficient in Eq. (5) which can analyze the matching conditions using Kroll's method [12].

$$\begin{aligned} &\cos(\Psi) = \frac{\sum(z)}{2} \\ &R \cdot e^{i\cdot 2\phi(z)} = \frac{2\sin(\Psi) - i \cdot \Delta(z)}{2\sin(\Psi) + i \cdot \Delta(z)} \end{aligned} \tag{5}$$

where $\sum(z) = \frac{E(z+L)}{E(z)} + \frac{E(z-L)}{E(z)}$, $\Delta(z) = \frac{E(z+L)}{E(z)} - \frac{E(z-L)}{E(z)}$. The distributions of R and the phase advance Ψ of the CLIC380 structure are plotted in Fig. 14(a) and (b), respectively, based on the ANSYS HFSS simulated field distribution along the beam axis given in Fig. 13(b) in conjunction with Eq. (5). In the matched case, the absolute value $|R|$ is less than 0.01 and the shift of phase advance Ψ error is 1°. In addition, the value of W_T obtained for the matched CLIC380 structure at $s = 0.15$ m (i.e., the position of two adjacent bunches) is less than 3.4 V/pC/m/mm, as required for ensuring beam stability. Moreover, F_{rms} is less than the required value of 5.

Note that an RF input power of 59.7 MW was required under the condition of beam loading to achieve $G = 72$ MV/m for the simulation model shown in Fig. 7. However, the required RF input power can be recalculated for the proposed tapered structure with couplers using the data given in Fig. 13(b). The simulated length of damping regular cells only, all cells and the entire structure are 258.3 mm, 275 mm and 295 mm, respectively. If the input RF power is 1 W, the acceleration voltages corresponding to these lengths are 3065.8 V, 3259.2 V and 3260.3 V, respectively. The data given in Fig. 11 can then be employed to calculate the voltage loss obtained under the condition of beam loading, which is 5.56 MV when $G = 72$ MV/m. Thus, the RF power under loading is 60.6 MW in the CLIC380 with a 275 mm active length. The average Q-factor of the overall CLIC380 structure can be calculated from the S12 parameters in Fig. 13(a) as about 5500, and the filling time becomes 56 ns, which is slightly greater than the previous value discussed in Section 4.

6. HOM damping loads

As discussed, the requirements of beam stability (i.e., beam dynamics (BD) requirements) in the CLIC380 design are that the transverse wake-field potential be suppressed to less than 3.4 V/pC/m/mm at $s = 0.15$, which is nearly two orders of magnitude less than the peak potential value. As a result, the entire CLIC380 structure, including the couplers, requires high-performance HOM damping loads to absorb HOMs. The distribution of HOM damping loads in the overall CLIC380 structure is illustrated in Fig. 15. Here, four equivalent HOM damping loads of an identical geometrical structure are applied at the same positions in every damping cell. However, HOM damping loads are not included within the coupling waveguide of couplers as Fig. 12(b).

In addition to the goal of absorbing HOMs to the greatest extent possible, it is equally important that the HOM damping loads absorb as little of the fundamental mode at $f = 11.994$ GHz as possible. For the CLIC380 structure, the cut-off frequency fc of the damping cells is about 14 GHz. This indicates that frequencies greater than fc are not appreciably attenuated by damping cells, while frequencies less than fc are attenuated. Thus, the fundamental mode at $f = 11.994$ GHz is

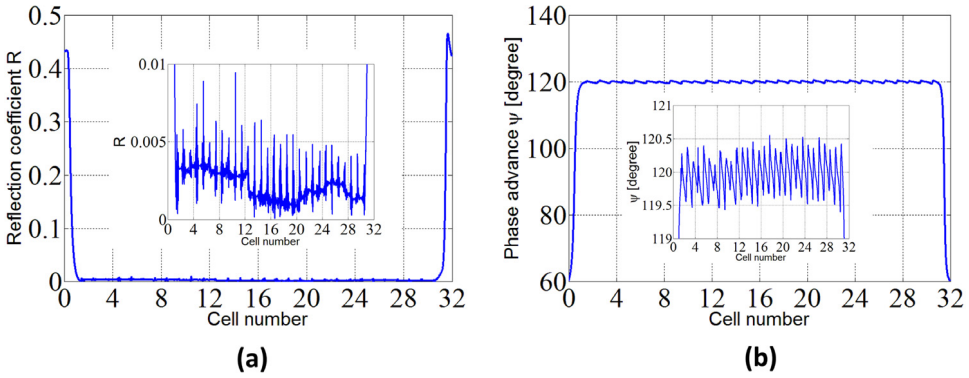

Fig. 14. Reflection coefficient (a) and phase advance (b) distribution of CLIC380 structure based on the simulated field distribution along the beam axis given in Fig. 13(b) in conjunction with Eq. (5).

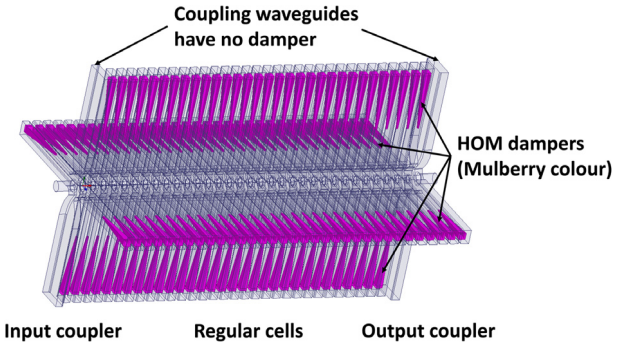

Fig. 15. Distribution of HOM damping loads in the overall CLIC380 structure.

attenuated in damping cells and propagated through the region that includes no damping waveguide cells. The electric field distribution of the fundamental mode is mainly concentrated in the central damping cells, and only a small fraction of that propagates through the waveguides. According to the relationship between the external quality factor Q_{ext}, internal quality factor Q_0 and loading quality factor Q_L, the difference between Q_L and Q_0 decreases with increasing Q_{ext}. The value of Q_0 corresponds to the power dissipated by the copper walls, and the value of Q_{ext} corresponds to the power dissipated by the HOM damping loads. Thus, it should be well done to absorb all HOMs and as little of the fundamental mode as possible.

As shown in Fig. 16(a), the HOM damping load is a smooth tapered box with a small cross-section at its tip, and the load is placed in the waveguide of a damping cell at a distance *Hd* between the center point of the beam aperture and the load tip. To increase the absorption of HOMs, the tip should be relatively small to reduce reflection, and the tapered box should be relatively long. The HOM damping structure is composed of SiC, owing to its advantageous complex permittivity [13]. As shown in Fig. 16(b), the extent to which the fundamental mode is attenuated depends on *Hd*. We note that a larger value of *Hd* is beneficial for maintaining a stable Q-factor by decreasing the power dissipation at the fundamental frequency, while a smaller value of *Hd* is desirable for ensuring a compact cell structure. Thus, an intermediate value of *Hd* is usually adopted to meet both requirements with reasonable effect. The optimum *Hd* results in Fig. 16(b) pertain to a value of *Hd* when the change in the Q-factor owing to the HOM damping structure is 1/10 000, which provides a power dissipation of −40 dB at the fundamental frequency. In this case, the HOM damping load mainly absorbs HOMs. The value of Q_0 is calculated at the copper boundary under a condition without damping load. The value of Q_{ext} is simulated by ANSYS HFSS with a perfect electric field boundary, such that power dissipation occurs only at the damping load.

For the optimum CLIC380 design, the distance *Hd* of the first cell, middle cell and last cell are 46 mm, 44 mm and 43 mm, respectively. The value of L_1 is 42 mm and the value of L_2 is 2 mm in the simulation. The maximum power loss on the copper wall of all cells is 1.2 MW, and the absorbed power of the fundamental mode for a single HOM damping load is less than 30 W because the power dissipation is inversely proportional to the Q-factor. The CLIC system operates at a 50 Hz repetition rate and the RF power pulse is 240 ns, which indicates that the average dissipation of a single HOM damping load is 0.36 mW. We plot the values of W_T simulated by GdifidL for the overall CLIC system, including HOM damping loads, couplers (Fig. 12) and damping cells (Fig. 7), in Fig. 17(a) using *Hd* = 44 mm for all cells. The use of HOM damping loads increases the long-range values of W_T relative to those obtained for the system composed of only damping cells and couplers. However, the values of W_T and F_{rms} remain less than their beam stability criteria values, as shown in Fig. 17(b).

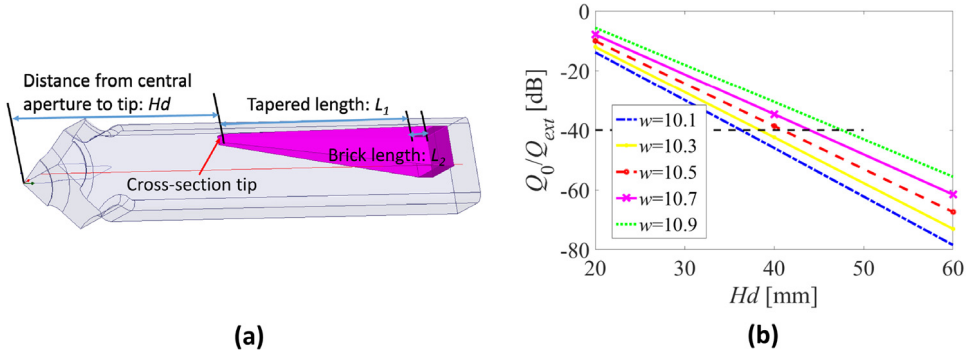

Fig. 16. (a) Geometry of a single HOM damping load in a waveguide of a quarter damping waveguide cell. (b) Power dissipation of the HOM damping load at the fundamental frequency versus the distance *Hd* from the central aperture of the damping cell to the load tip.

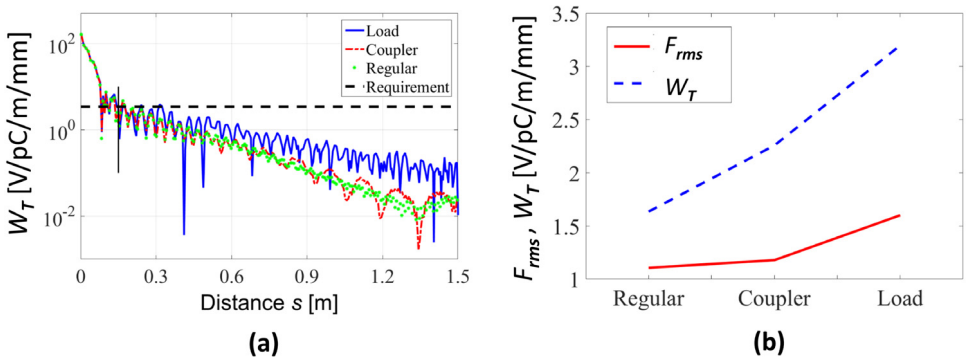

Fig. 17. Values of W_T for the HOM damping load design of the CLIC380: (a) HOM damping load of Fig. 15 (blue), coupler model of Fig. 12 (red), damping waveguide cells of Fig. 7 (green); (b) W_T and F_{rms}.

7. Summary

This work presented an optimized design for the 380 GeV high-gradient RF acceleration structure stage of the CLIC to ensure a high RF-to-beam efficiency. The parameters *iw* and *w* of the damping waveguide cells were optimized to reduce long-range transverse wakefield potentials below the beam stability requirement of 3.4 V/pC/m/mm at the bunch separation distance. In addition, linearly decreasing values of *iw* were applied to the sequence of damping waveguide cells with respect to the direction of beam propagation to reduce the maximum value of ΔT in the last cell to <40 K. Meanwhile, the eccentricity of the iris and the wall profiles were optimized to further minimize ΔT and the magnitude of *Sc*. The couplers were well matched to meet the requirement of low reflection. With all the above geometrical improvements, the transverse wakefield enhancement factor F_{rms} remains less than 1.2. The effect of reducing the value of *Hd* was also studied to make the damping waveguide structure more compact. The simulated wakefield suppression obtained with HOM damping loads was slightly less than that obtained with ideal condition of complete absorption in damping loads, but the design targets were still satisfied.

Acknowledgments

Authors are grateful to H. Zha for his assistance during the research. Thanks to the help and support of people from European Organization for Nuclear Research and Shanghai Institute of Applied Physics, Chinese Academy of Sciences.

References

[1] CLIC Conceptual Design Report (CDR), 2012, http://project-clic-cdr.web.cern.ch/project-CLIC-CDR/CDR_Volume1.pdf.
[2] Updated Baseline for a staged Compact Linear Collider, 2016, http://dx.doi.org/10.5170/CERN-2016-004.
[3] W.C. Fang, D.C. Tong, Q. Gu, et al., Design optimization of a C-band traveling-wave accelerating structure for a compact X-ray Free Electron Laser facility, Chin. Sci. Bull. 56 (2009) 3420.
[4] W. Wuensch, High-gradient acceleration: CLIC and beyond. Talk in 2016, CLIC workshop, Geneva, Switzerland, 2016.
[5] A. Grudiev, S. Calatroni, W. Wuensch, New local field quantity describing the high gradient limit of accelerating structures, Phys. Rev. Accel. Beams 12 (2009) 102001.
[6] H. Zha, A. Grudiev, Design and optimization of Compact Linear Collider main linac accelerating structure, Phys. Rev. Accel. Beams 19 (2016) 111003.
[7] Ansys HFSS, http://www.ansys.com.
[8] W. Bruns, http://www.gdfidl.de.
[9] H. Zha, W. Wuensch, D. Schulte, et al., Beam-based measurements of long range transverse wakefields in CLIC main linac accelerating structure, Phys. Rev. Accel. Beams 19 (2016) 011001.
[10] D. Schulte, Multi-bunch calculations in the CLIC Main LINAC. Proceedings of PAC09, Vancouver, BC, Canada, 2009, FR5RFP055.
[11] X.X. Huang, A. Grudiev, RF design and parameters of 12 GHz prototype TD31_vg2.9_R1_CC, https://edms.cern.ch/document/1772531/1.
[12] N.M. Kroll, et al., Applications of time domain simulation to coupler design for periodic structures. SLAC Pubs and Reports, Menlo Park, CA, USA, 2000, SLAC-PUB-8614.
[13] G. De Michele, Wakefield Simulations and Measurements for the CLIC RF Accelerating Structure (Ph.D thesis), École Polytechnique Fédérale de Lausanne, 2014.